High conversion efficiency microscopic tin-doped droplet target laser-plasma source for EUVL

Chiew-Seng Koay, Simi George, Kazutoshi Takenoshita, Robert Bernath, Etsuo Fujiwara**,
Martin Richardson*, Vivek Bakshi***
Laser Plasma Lab, College of Optics: CREOL & FPCE,
University of Central Florida, Orlando, FL 32816

ABSTRACT

Light sources based on laser plasmas using tin as target material are known to provide high conversion efficiency of laser power to emission in the 13.5 nm spectral region. In addition, laser plasmas produced from microscopic droplet targets enable the utilization of the mass-limited concept which minimizes the effect of target debris produced from the laser plasma interaction. By combining the mass-limited target concept and tin as the choice of target material, we are developing an extreme-ultraviolet (EUV) light source that can supply high power while remaining essentially debris-free. This source uses tin-doped microscopic droplet liquid targets that are generated at high-repetition rates (>30 kHz), which allows convenient upward power scaling when coupled with a high averaged-power laser.

Detailed studies of the radiation from this source have been made using a precision Nd:YAG laser. Broad parametric studies of the conversion efficiency along with in-band spectroscopy of this EUV source have been performed. The parametric dependence of conversion efficiency is established based on measurements made by the Flying Circus diagnostic tool and a calibrated high-resolution flat-field spectrometer. These measurements have been independently confirmed by the Flying Circus 2 team.

Keywords: EUV, sources, laser-plasmas, tin plasmas

I. INTRODUCTION

There is a concerted international effort at present in the development of EUV lithography (EUVL) as a technology for the fabrication of next-generation computer chips. The development of a high power EUV light source having the emission lifetime and cost-model requirements for EUVL remains one of the principal challenges. Both laser plasma and the discharge plasma sources are being developed to meet this need: a stable, debris-free light source combined with suitable collection optics that can provide useful EUV radiation power above 115 W at the so-called intermediate focus [1], which is located at the entrance of the illumination optics of the EUV lithography stepper. The power level is based on a number of assumptions including a photo resist sensitivity of 5 mJ/cm^2 for 300 mm diameter wafers, imaging mirrors with reflectivity > 67% at 13.5 nm with a 2% spectral bandwidth, and a processing rate of 100 wafer layers per hour (wph).

Laser plasmas, in principle, have many attractive features for application in EUVL. Since the laser energy is delivered to the source by optical coupling, the laser and its associated infrastructure can be located separate from the stepper, unlike a discharge source, which requires much of its cooling and power system to be integral. Depending on geometry and laser architecture, a laser-plasma source can easily extend to greater dose stability because the source's repetition rate increases conveniently beyond 10 kHz. Moreover, laser-plasmas provide a wide margin on the source size requirement for EUVL. Since all EUV steppers are expected to have etendue in the range of 1 - 3.3 mm^2·sr, this implies a limit of the source size to be < 1 mm. The source sizes of discharge sources are likely to exceed this limit as their power levels are pushed higher to meet the overall power requirement. Since the laser-plasma source size is considerably smaller than that of discharge sources, it can achieve higher power operation through increased repetition-rates with less chance of overstepping the etendue limit.

---

*email: mcr@creol.ucf.edu, Fax: +1-407-823-3570
** Present address: Himeji University, Japan, *** SEMATECH, 2706 Montopolis Drive, Austin, TX 78741

For a laser-plasma source to succeed, it must meet very high performance levels at 7 - 10 kHz operation with a pulse-to-pulse energy stability <2%. In addition, the source must work in a scheme that can prevent the collection optics from suffering the deleterious effects of target debris. Apart from the strict condition of debris-free operation of the source, the conversion efficiency (CE) of the source into useful EUV power becomes an important parameter to be optimized. For a laser plasma source, the CE must be sufficiently large to (i) provide the projected required collectable power levels with viable commercial lasers and (ii) permit the overall cost of the source, including the laser, to remain within economic models of the overall EUV lithography stepper tool.

The EUV spectrum of the light emitted from the hot dense plasma depends strongly on the material from which the plasma is created. Plasmas of materials from high-Z elements that are located from V to VII in the p-block of the fifth period of the periodic table are advantageous for efficient radiation about 13.5nm [2]. Laser plasma sources that uses tin (Sn, atomic number = 50) as the target material are known to provide high conversion efficiency for in-band emission at 13.5nm since the early studies with solid tin target [3, 4]. However, the material was thought unsuitable for EUV lithography because of the debris it produces when used in conventional metallic form.

This has led to the utilization of xenon as a target material in both the laser-plasma and the gas-discharged plasma, as well as the development of laser-plasma sources based on mass-limited target. At present, most of the EUV source developers are using xenon [5]. The material was favored over metal tin because of the notion that the inert gas has a better potential to succeed as a debris-free EUV source, although for xenon, only one ion stage (Xe^{10+}) [6-8] within the plasma effectively contributes to the in-band emission at 13.5 nm as compared to tin, which has many [2, 9-11]. Although much effort have been placed in trying to improve the CE, the value remains <1.0% into (2%BW $\times$ 2π $\times$ sr) [12-15]. In addition, debris issues related to sputtering by energetic xenon ions remains to be solved [13-17].

A number of laser plasma schemes have been investigated [18-31] for EUVL. They include the high density, pulsed or continuous cluster targets, liquid jets or liquid droplets targets of xenon and/or water. Since 1992, we have been investigating laser-plasmas based on the mass-limited targets [18-23], which lead to low debris operation, by using targets created in the form of microscopic liquid droplets. The targets have demonstrated extended operating lifetimes without significant debris contamination [21]. Unfortunately, to date, both the xenon and the water laser plasma sources showed conversion efficiencies of <1.0%, a value that makes achieving the requirement for sufficient power for EUV lithography difficult with the available laser technology.

We are currently developing a laser-plasma light source that can supply high power in EUV radiation while remaining essentially debris-free. Our approach incorporates the use of tin with the mass-limited concept, which we have extensively investigated, to develop the tin-doped micro droplet targets [10, 11, 32-35]. The advantage of our approach is evident resulting in recent developments of target schemes of the similar concept [36, 37]. In addition, as the deadline for EUVL implementation in high volume manufacturing is approaching, there have been considerations [38]made by source developers in the early 2003 concerning switching the source material from xenon to tin, or adding tin to the existing xenon scheme, in an attempt to improve the EUV output.

Here we report the progress of our studies on the tin-doped micro droplet target laser-plasma source which demonstrates in-band CE in excess of 2%. With this value of CE, and assuming 50% throughput for the collection optics, powers at the intermediate focus of approximately 50W can be obtained with currently expected high power solid state Nd:laser technology [39]. Section II of the paper discusses the laser interaction with spherical micro targets, including the hydrodynamic code simulations of electron temperature and density of the plasma. The experimental facility for characterization of the 13.5nm emission is described in Section III. In Section IV, we report spectroscopic studies of the source by examining the spectra due to the effects of laser intensity, and laser spot size. The last section is on calibrated metrology at 13.5 nm in which a detailed method for determining CE is explained. We report results on the studies of the CE as a function of a wide range of laser intensities through which the optimum intensity for maximum CE was determined. Detailed quantitative studies of the debris and development of debris mitigation techniques for the source are reported in Refs. 33 and 34.

II. LASER INTERACTION WITH SPHERICAL MICRO TARGETS

The interaction of a high intensity laser pulse with a micro target involves complex hydrodynamics and atomic processes. During the interaction of a laser pulse with the spherical target, the most efficient mechanism for transferring the laser energy to the plasma is through the inverse *Bremsstrahlung* absorption. In this process, electrons that have been ionized from the target's material oscillate under the action of the laser's electric field, and collide with the ions to transfer the electromagnetic wave energy to the plasma.

Radiation from hot dense plasma is emitted via free-free, free-bound and bound-bound mechanisms. The first mechanism gives rise to a continuum electromagnetic spectrum when free electrons in the plasma interact with the Coulomb potential of the ions. The second mechanism produces also a continuum spectrum when free electrons recombine with ionized atoms. Line emission is produced from the third mechanism as a result of transitions between discrete levels of ionized atoms.

Hot dense plasma created from high-Z materials commonly has many ion stages that can radiate line emission, and when these strong lines superpose in energy within a localized spectral region, they form characteristic spectral features. It is sometimes difficult to assign any characteristic wavelength to the lines within the spectral feature as a whole because (i) there too many lines to identify the individual transitions and (ii) the individual lines cannot be resolved within the limits of spectrographic instrument. Known as the unresolved transition array (UTA), [40] the spectral features in the EUV region emitted by plasma of various elements have been studied [41, 42]. The most prominent UTA of tin and xenon targets in the EUV region are located at ~13.5nm [2, 9, 11] and 11nm respectively [7, 8].

The radiation emitted from laser plasma depends strongly on the plasma conditions such as electron temperature and electron density, which are influenced by various laser and target parameters on plasma heating. Simulations using laser plasma codes provide useful information about the plasma dynamics to find an optimum laser and target parameter where the useful EUV radiation is produced most efficiently. We have been employing the one-dimensional hydrodynamic simulation code MEDUSA 103 for this purpose [43]. The code allows the user to adjust various laser and target parameters: laser pulse duration, intensity, wavelength, pulse shape, target atomic mass and composition, to model the electron density, electron and ion temperature, plasma velocity, average ion charge state, as a function of time and space. The laser parameters used in the calculations are the same as the laser used in experiments, which will be described in detail in the next section. In the simulation, the parameters used are: 11ns pulse width at 1064nm wavelength. The target is a spherical droplet containing tin material. The range of laser intensity at the target region in the studies is $10^{10} - 10^{12}$ W/cm^2.

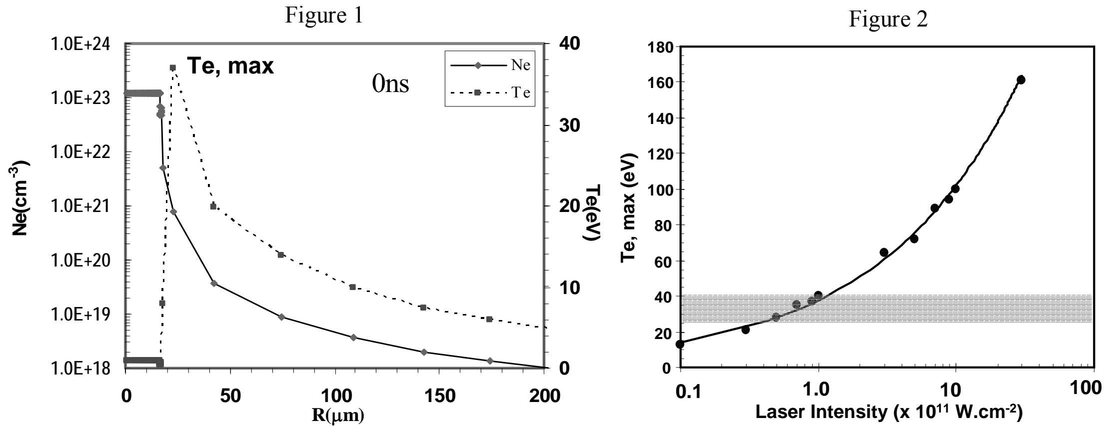

Figure 1: Typical simulation result for tin-doped droplet target, showing the electron temperature and density at a time corresponding to the peak of the laser pulse. Figure 2: The maximum T_e as a function of laser intensity as predicted by MEDUSA, for a spherical target of 35μm in diameter and containing 30% tin by mass.

Figure 1 shows a typical simulation result for a tin-doped target of spherical geometry (35 μm diameter and having 30% tin by mass). It shows the variation of the predicted electron temperature and electron density in space, for a time corresponding to the peak of the laser pulse. The horizontal axis is the distance measured from the center of the target. The simulation shows that by the time the laser pulse reaches this peak intensity, the absorption region of the plasma, primarily due to inverse *Bremsstrahlung* absorption, located at distances from the center of the target that are below the critical electron density (10^{21} cm^{-3}) has expanded to completely fill the laser spot size, which varies from 35μm to 100μm in diameter. Also, the electron temperature reaches a maximum value around that same region.

A series of simulations was made to observe the dependence of the predicted maximum electron temperature as a function of laser intensity for the tin-doped droplet target laser plasma source using a particular target parameter: 35μm diameter spherical target with concentration 30% tin by mass. Results were obtained for laser intensities ranging from 1 x 10^{10} to 3 x 10^{13} W/cm^2, as shown in Fig. 2, where the dependence of $T_{e,max}$ and intensity is a rather smooth function. The Cowan code [44] calculation of the Sn ion stages distribution at electron density of 10^{21}cm^{-3}, as a function of electron temperature, is shown in Fig. 3. The result predicted that optimum production of the 13.5 nm UTA occurs in the range of electron temperature around 30eV, when the relative abundance of Sn^{9+}, Sn^{10+}, and Sn^{11+} are dominant Around that electron temperature, the results from MEDUSA indicate that the laser intensity for optimum EUV emission would be located around 1.0 x 10^{11} W/cm^2, for this particular target parameter. This predicted region for optimum emission lies within the shaded box in Fig. 2.

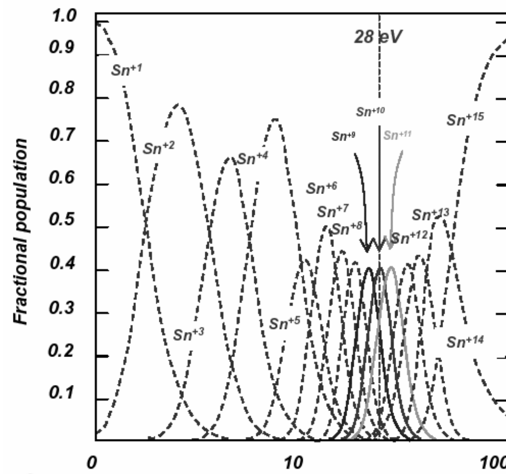

Figure 3: Sn ion distributions as function of electron temperature (in eV) calculated from Cowan code for electron density at 10^{21}cm^{-3} [45]

These results provide helpful insight for the experimental work in developing an efficiency laser plasma source for EUV lithography. Section V presents the experimental results of conversion efficiency as a function of laser intensity and compares with theoretical predictions.

III. EXPERIMENTAL CHARACTERIZATION OF 13.5nm EMISSION

The Laser Plasma Laboratory's facility for studying EUV radiation consists primarily of a precision Nd:YAG laser, a target vacuum chamber and various EUV diagnostics. The cylindrical target chamber consists of 12 vacuum ports that are positioned around the body of the cylinder, allowing various EUV diagnostics to be connected to the chamber. The axes of all the ports intersect at the center of the chamber, where usually the target is positioned during an experiment. Fig. 4 shows the experimental setup, depicting a flat-field spectrometer and a Flying Circus [46] instrument positioned at angles 90° and 30° respectively from the input laser beam axis.

A light-valve assembly consisting of a half-wave-plate and Glan-laser polarizer was used to adjust the laser pulse energy. An optical-flat sampled off the laser beam to be measured with a fast photodiode. Prior to an experiment, the signal

from photodiode was calibrated against an energy meter that was placed after the focus lens in the target chamber. The linearity of the photodiode signal was checked by varying the laser energy across the range of interest for the experiment.

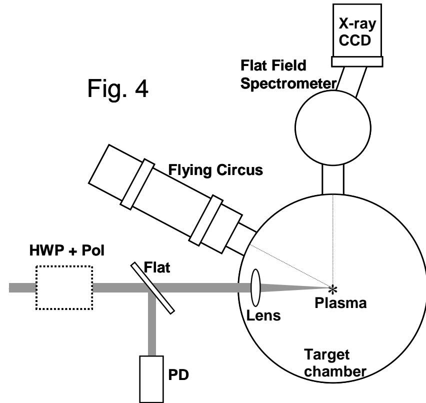

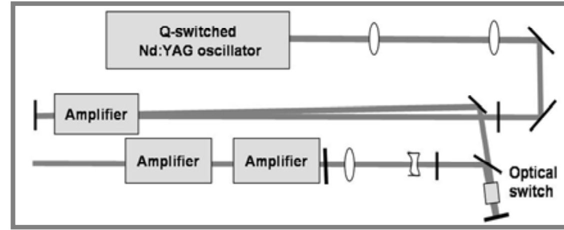

Figure 4: Experimental setup for radiation studies. PD is photodiode whose signal has been calibrated against an energy meter placed at the target. HWP + Pol is a light-valve assembly consisting of a combination of a half-wave-plate and a Glan-laser polarizer.
Figure 5: Optical layout of the precision Nd: YAG laser.

The laser used in the studies is a precision Q-switched Nd:YAG oscillator-amplifier laser system (λ = 1064 nm) operating at 1Hz, producing up to 1.6J energy per pulse, with a 11.5 ns (FWHM) pulse duration. The laser consists of a master oscillator and three amplifier modules (Fig. 5). The laser beam makes two passes through the first amplifier, followed by single pass through the remaining amplifiers. The beam quality of laser output has an M^2 ~1.5 and a Gaussian fit correlation ~0.93. A minimum spot size of 35 μm diameter is achievable when the laser beam was focused by an f = 10cm plano-convex lens. Fig. 6 shows the far field beam profile recorded by using a laser beam analyzer, and a detailed map of the focal region when using the f = 10 cm lens.

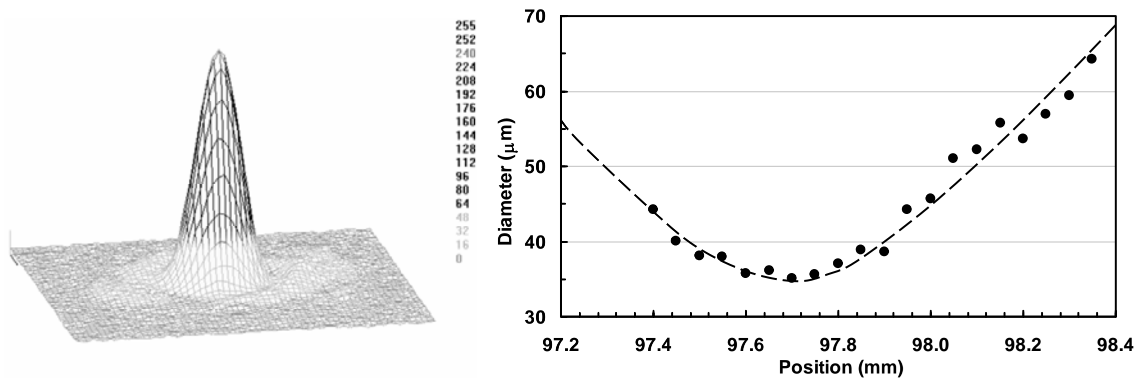

Figure 6: Laser beam performance showing a far-field beam profile that is Gaussian in shape and the detailed map of the focal region for an f = 10cm lens.

A. Diagnostics

High resolution spectroscopic studies of the EUV emission from the source were performed using a flat-field grazing incidence grating spectrograph. The flat-field spectrograph (FFS) uses a 1200 lines/mm, gold coated, variable spaced reflective grating in a configuration reported previously [47]. An entrance slit is used to collimate the light from the source to the grating with 3 degrees grazing incidence angle. The slit-to-grating and grating-to-image-plane distances are 237 mm and 235 mm respectively. A 0.5 μm thick, freestanding Zr metal filter is used in the spectrometer to select

wavelengths from 6.5 – 16.8 nm (FWHM). A back-thinned x-ray CCD camera is used to record the dispersed spectrum [48].

Although the laser plasma source emits a range of radiation, from the visible to the x-ray, only those within a 2% bandwidth located at 13.5nm is useful for EUV lithography. The amount of energy emitted from the source, within this spectral band, is measured with the so called Flying Circus (FC) instrument [46]. The FC is a narrowband EUV diagnostic comprising a calibrated curved normal incidence multilayer mirror and a Zr filtered AXUV–100 photodiode [49]. The Mo-Si multilayer spherical mirror collects light from the source; a fresh mirror typically has a peak reflectivity of 69% at 13.5 nm and a narrow reflectivity band (~3.7% FWHM). The photodiode has a spectral responsivity of 0.23 A/W at 13.5 nm, and it is operated with a reversed bias at 26 volts to ensure linearity. The transmission at 13.5 nm for a 0.5 μm thick Zr metal filter is ~18% [50]. Calibration of the optics used in the diagnostics employed in studies presented in this paper was made by NIST.

B. Mass-limited target

To minimize the effects of target debris produced from laser plasma interaction, we utilized the concept of mass-limited target. This concept aims toward limiting the mass of the target to one whose mass, and size, approximates that of simply the number of atomic radiators required for emission. In this way, the number of neutral target atoms generated can be controlled, and the production of high velocity solid particles emanating from the target can hopefully be avoided completely.

The targets are produced in the form of small spherical droplets ~35 μm diameter, with a small amount of tin mixed in low-Z material. The amount of tin in each droplet target is in the order of 10^{13} tin atoms, and the number can be controlled by changing the target composition. These tin-doped droplet targets are produced from a capillary dispenser. When driven through a nozzle by a piezo-electric module at a high frequency, a thin chain of droplets is produced (Fig. 7). Generating the droplets at high rate of 20 - 200 kHz is advantageous because, if each droplet is heated by a laser pulse from a high averaged-power laser to produce EUV, then the emitted power can conveniently be scaled upward to meet the power requirement for EUV lithography. When the source is in operation, each target is synchronized to a laser pulse so that the positional stability of the high velocity (typically 2 x 10^4 cm/s) droplet target in the target region is about 3 μm at distances of 10mm from the nozzle's exit.

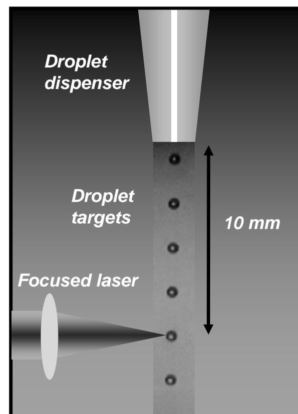

Figure 7: Photograph of a thin chain of droplet targets together with a cartoon of a laser beam focused on a droplet.

During experiments, the target was located centrally in the 45 cm diameter target chamber, which was operated in vacuum at pressure below 10^{-3} Torr with a turbo-drag pump that was backed with a roughing pump. At this pressure, absorption of EUV radiation by the air inside the target chamber is <1% for a distance of 100 cm [50].

IV. SPECTRAL CHARACTERISTICS OF THE EUV EMISSION

A. Intensity dependence

An experiment was performed to record spectra from the tin-doped droplet target laser plasma as a function of laser intensities at the target, ranging from $10^{10} – 10^{12}$ W/cm^2. From the point of view of designing an efficient EUV source, the goal of this study is to identify the tin ion species that are responsible for contributing toward the useful spectral band as well as to determine any spectral signature that may exist in relation to the optimum irradiation condition.

The target material contained 30% tin by mass. The concentration is quoted as "% tin by mass", which is equal to the mass of tin in the target divided by the total mass of the target. The droplet dispenser was setup to allow the droplets to fall vertically to the center of the chamber. While the incident laser pulse energy was kept constant, the laser intensity irradiating the target was varied by defocusing the lens to change the laser spot size irradiating the target. The amount of defocus was controlled by a precise mechanical adjuster which controls the distance between the lens and the target. Since the laser spot size is known from the detailed map at the focal region (Fig. 6), the intensity can be determined accurately.

The FFS was aligned to the position of the source and it was connected to the target chamber as shown in Fig. 4. The entrance slit width of the FFS was 117μm, and the source-to-slit distance was 395mm. For each laser intensity setting, a spectrum was recorded by the x-ray CCD camera exposed over the duration of 20 laser shots. A computer program was developed to analyze the spectra. Through a deconvolution process, the raw spectra recorded by the x-ray CCD were converted to their true spectra by removing the effects from the Zr filter's transmission.

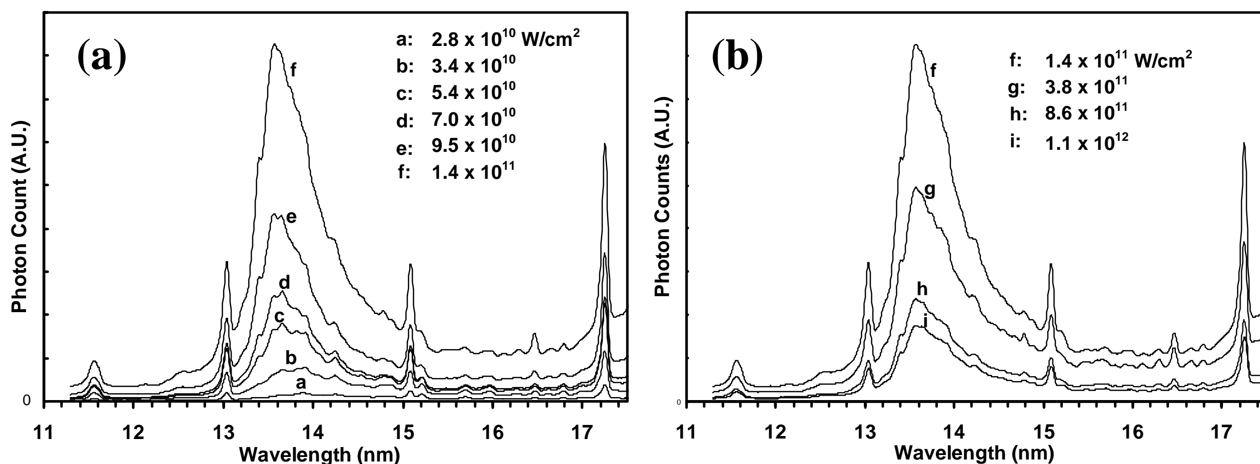

Figure 8: (a) Spectra from tin-doped droplet target laser plasma for various laser intensities below 1.4 x 10^{11} W/cm^2 at the target. and (b) Spectra from tin-doped droplet target laser plasma for various laser intensities above 1.4 x 10^{11} W/cm^2 at the target.

Figures 8 (a) and (b) show that the peak of the tin UTA at 13.5nm, which has a narrow width of 1nm (FWHM), increased in height with intensity until a particular intensity, after which the peak decreased. This UTA arises primarily due to $4p^6 4d^N \rightarrow 4p^5 4d^{N+1} + 4p^6 4d^{N-1} 4f$ transitions from Sn^{8+} to Sn^{11+} ion stages overlapping in energy [2]. In this series of spectra, the intensity at which the tin UTA reaches the maximum height (spectrum **f**) is 1.4 x 10^{11} W/cm^2. This intensity, which will be referred to as the optimum intensity because it is found to correspond to the maximum CE, is consistent with the prediction provided by the hydrodynamic code. Its relation to conversion efficiency will be presented in more detail in later section.

To observe the effects that the laser intensity has upon the structures within the UTA, the spectra were normalized to the peak of the oxygen lines (13.0nm and 15.1nm) that appear in the spectra. Figures 9 (a) and (b) are the spectra after normalization. Below the optimum intensity, the spectra show that there are at least four features (approximately denoted by dotted lines I, II, III and IV) within the UTA that respond sensitively to the laser intensity. A significant increase in

emission near 13.5nm, mainly due to features I and II, was observed as the intensity increases. This can be explained from the fact that there was an increase in the relative abundance of Sn ion stages that emit into this wavelength. The Cowan code predicted (Fig. 2) that the optimum electron temperature is around 30eV, at which Sn^{10+} is dominant among the other ions contributing to the UTA, i.e. Sn^{6+} to Sn^{13+}. Therefore, to maximize the conversion efficiency, it is imperative to find the condition for maximizing the line emissions contributing to spectral region of interest.

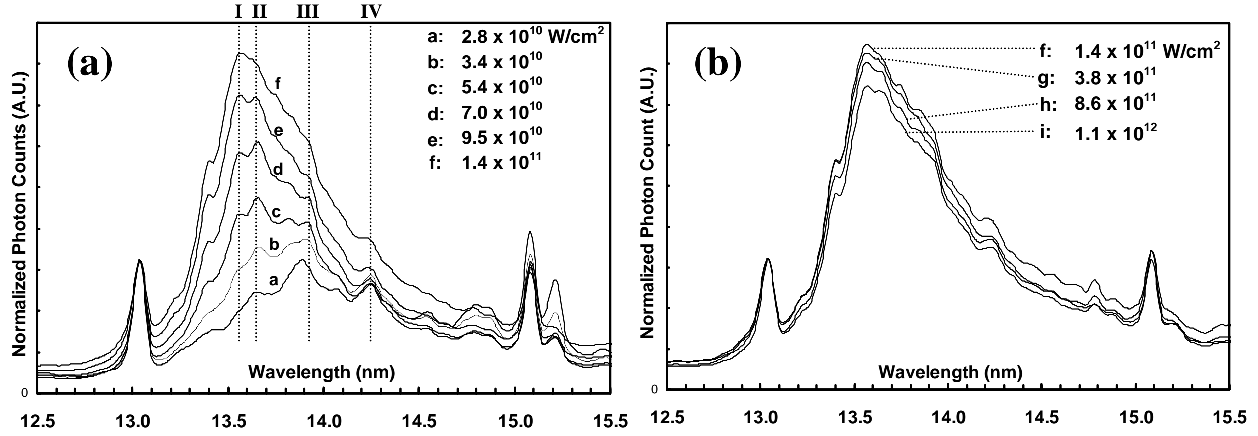

Figure 9: (a) Spectra that have been normalized to the peak of the oxygen line (at 13.0nm) for various intensities < 1.4×10^{11} W/cm^2. Dotted lines I, II, III, and IV denotes the spectral features that respond sensitively to the variation in laser intensity. and (b): Spectra that have been normalized to the peak of the oxygen line (at 13.0nm) for various intensities > 1.4×10^{11} W/cm^2. The shape of the UTA, at the various intensities, remains the same.

From these results, the laser intensity for the plasma to emit the maximum useful EUV is found. In addition, the tin ions responsible for producing features I and II are most likely from Sn^{8+} - Sn^{10+} for the following reason. While the intensity was increased toward the optimum value, so does the electron temperature, during which the dominant tin ionization stage shifted from Sn^{6+} to Sn^{10+}, causing the spectrum to change from **a** to **f**. Spectrum **f** was produced at the optimum intensity condition, when features I and II are dominant. In comparison, spectrum **a**, which was produced at an intensity considerably smaller than the optimum, but enough to enable emission toward the tin UTA, has features III and IV more dominant than the rest. Since spectrum **f** was recorded at the optimum condition, which according to the Cowan code prediction, when ion Sn^{10+} is dominant, it is reasonable to attribute features I and II to be largely due to ions near Sn^{10+}.

Above the optimum intensity, the peak of the UTA dropped (Fig. 8(b)), indicating that there are lesser ions emitting into the UTA. This is understood as a result of the increased electron temperature at higher intensity creating more ions of higher ionization stages, thus reducing the ion population of those that emit into the UTA. Although the change in the spectral peak was substantial, Fig. 9(b) shows that the overall UTA shape remains unchanged with increasing intensity. This suggests that the distribution of Sn ionization stages, of those that contribute to the UTA, remains unaffected.

B. Spot size dependence

In the same experimental run, another set of spectra was recorded to observe whether the laser's spot size affected the intensity dependence of the spectra. In these measurements, the variation in intensity was made by keeping the laser spot constant in size, while the laser pulse energy was varied. The lens was fixed at the position where the spectrum **f** was recorded. At this position, the laser spot size on the target was 100 μm in diameter. The input laser pulse energy was varied by rotating the half-wave-plate, as shown in Fig. 4. The result of the measurements for intensities < 1.4×10^{11} W/cm^2 is shown in Fig. 10. When it is compared with Fig. 9(a), the two are essentially the same, implying that the laser spot size has negligible effect on the UTA's intensity dependence. The spectra recorded for intensities >1.4×10^{11} W/cm^2 also give the same conclusion.

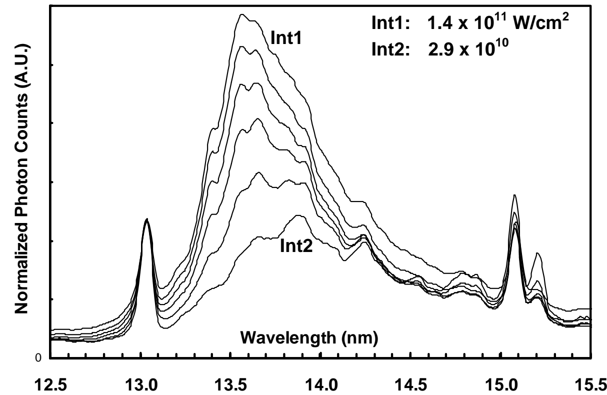

Figure 10: Normalized spectra for laser intensities between 2.9 x 10^{11} and 1.4 x 10^{11} W/cm^2 recorded with constant laser spot size.

V. CALIBRATED METROLOGY OF 13.5nm EMISSION

A. Method of CE measurement

The standard way for measuring absolute in-band EUV energy emitted from a plasma source is by using an instrument with calibrated EUV optics. In our studies, the Flying Circus instrument was utilized and the optics in it was calibrated by NIST.

In a long running experiment, especially when many energy measurements must be made for a wide range of irradiation conditions, there arise a concern about maintaining the calibration of the Mo-Si multilayer mirror, whose reflectivity is sensitive to effects from target debris on its multilayer coating, from changing throughout the duration of the experiment. To avoid this problem, a FFS was added to the experimental setup and used together with the FC. Together, a spectrum and an energy measurement could be obtained simultaneously for a particular irradiation condition. Then, the spectrum was calibrated against the corresponding energy measurement made by the FC. The CE calculated from this measurement can then be characterized by its spectrum, and it served as a reference value for calculating the CE for other irradiation conditions whose spectra were recorded. Thus the FC was used to make only one measurement in an experiment, thus preserving its pristine calibration. The FFS was then used as a calibrated instrument for measuring CE. Since the instrument has a collimating slit and a Zr filter placed in between the source and its grazing incidence grating, the effects from target debris on the instrument's calibration would be minimal throughout a long running experiment. Another advantage for using the FFS for energy measurement was because it allowed precise CE calculation for all irradiation conditions. The reason for this, as will be seen later, is due to the fact that a spectrum is needed for calculating the CE. Since the spectra vary with changes in the irradiation condition, as was seen the previous section, then the CE is calculated corresponding to its spectrum for that particular irradiation condition.

B. Reference parameters and conversion efficiency

The experimental setup for measuring the CE as a function of laser focus position, and as a function of laser intensity, is shown in Fig. 4. The plasma was created with the precision 1-Hz laser. A spectrum was recorded over the duration of 20 laser shots and simultaneously an energy measurement was made with the FC.

An advantage for using the 1 Hz laser in making CE measurements was that it allowed precise determination of the EUV energy for each input laser pulse energy, since at such a low repetition rate, the pulse to pulse energy can be observed rather easily by using the following method. A fast photodiode which has been calibrated was used to measure the energy of the input laser pulse. The signal from the photodiode and the EUV signal from the FC were connected to a high speed oscilloscope, so that both signals appeared simultaneously on the oscilloscope's screen. Over the duration of the 20 shots, a webcam, to which the oscilloscope's screen was imaged, was used to record a video of the two signals. A snap shot of the video is shown in Fig. 11.

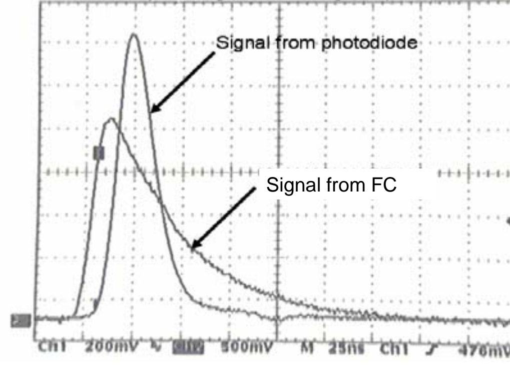

Figure 11: A photograph of the screen of an oscilloscope that contains the signal from the photodiode and the signal from the FC instrument. The laser pulse duration is actually 11.5ns (FWHM) but was broadened due to the reduced sampling bandwidth (20MHz) setting.

From Ref. 51, the EUV energy radiated by the source over 2π steradian solid angle and within a 2% bandwidth centered on 13.50nm, is given by

$$E_{BW} = \frac{2\pi}{\Omega R_{scope}} \left(\frac{\int_{BW} I_s(\lambda) d\lambda}{\int_{all} I_s(\lambda) R_{mir}(\lambda) T_g(\lambda) T_f(\lambda) \eta_{diode}(\lambda) d\lambda} \right) A_{scope} \tag{1}$$

where Ω is the collection solid angle of the FC mirror subtended from the source, A_{scope} is the integrated area under the EUV signal waveform displayed on an oscilloscope, R_{scope} is the impedance of oscilloscope channel, $T_g(\lambda)$ is the transmission curve of the gas in the vacuum chamber (from CXRO), $R_{mir}(\lambda)$ is the calibrated mirror reflectivity curve, $T_f(\lambda)$ is the transmission curve of filter(s) used to block visible light from entering AXUV detector, $\eta_{diode}(\lambda)$ is the calibrated responsivity curve of the AXUV detector in the FC, and $I_s(\lambda)$ is the spectrum of the EUV source in arbitrary units.

Equation 1 assumes isotropic emission from the source. The method used for calculating CE is the same as the method employed by the FC2 team, which is mentioned in Ref. 51. A numerical analysis program was developed for this purpose. The program takes a number of input files (i.e. the spectrum and the optics calibration files). Then a process of interpolation was carried out in the program to combine the related input files, and finally the program performs numerical integrations to calculate the source's EUV energy. In the numerator, the limits of integration for the 2%BW (centered at 13.50nm) are from 13.365nm to 13.635nm. Although the integral in the denominator is over all wavelengths, in practice, it is integrated only over the region where the integrand contributes significantly, which is generally determined by the product of $R_{mir}(\lambda)$ and $T_f(\lambda)$. The CE then is the ratio of the E_{BW} to the laser energy at target. As a standard, the CE is quoted in the units of "percent over 2π str × 2%BW at 13.5nm".

Because of the fact that

$$A_{scope} \propto \int_{all} I_s(\lambda) R_{mir}(\lambda) T_g(\lambda) T_f(\lambda) \eta_{diode}(\lambda) d\lambda \,, \tag{2}$$

it provides a way to relate the spectrum and E_{BW} using the following expression

$$E_{BW} \propto \int_{BW} I_s(\lambda) d\lambda \,.$$

Consequently this allows the FFS to be calibrated against the FC. A set of reference parameters is created from the reference measurement. Many spectra were recorded during an experiment, in which a spectrum was recorded for each

irradiation condition. Corresponding to each irradiation condition are its spectrum $I_{s,i}$ and input laser energy $E_{L,i}$. The CE for that irradiation condition is then obtained from

$$CE_i = \left(\frac{\int_{BW} I_{s,i}(\lambda) d\lambda}{\int_{BW} I_{s,ref}(\lambda) d\lambda} \right) \left(\frac{E_{L,ref}}{E_{L,i}} \right) CE_{ref} \qquad (3)$$

B. Conversion efficiency dependence on focal position

An experiment was performed to measure CE as a function focus position. The tin-doped droplet target contained 30% tin by mass. In this experiment, the laser pulse energy was set constant at an average value of 60 mJ. Then, the separation distance between the target position and the minimum focus position of the laser beam was varied by translating the position of the focusing lens along the laser axis. The unit step of separation was 200 µm. The position scan was made from one side of the focus to the other side, passing the minimum focus. An energy measurement was made with the FC and simultaneously a spectrum was recorded with a 20 s exposure corresponding to 20 laser shots from the 1 Hz laser. From this particular energy and spectrum measurement, a reference CE was obtained using the abovementioned method. Then, at each subsequent separation distance, a spectrum was recorded with the same amount of exposure. Figure 12 shows that result of the experiment. The position of the dip in CE is where the minimum focus of the laser was located. In this experiment, higher CE was obtained when the target was placed at some distance from the minimum focus.

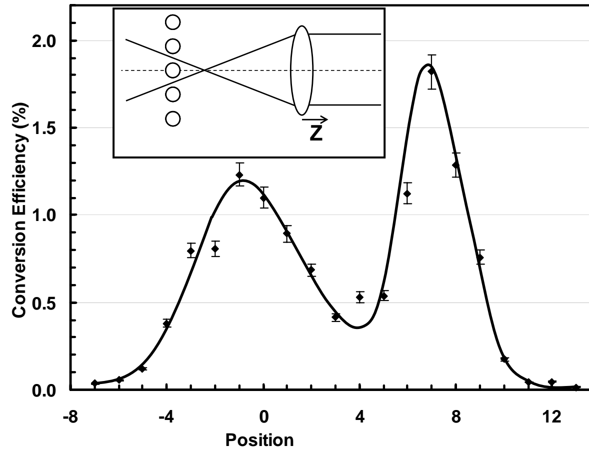

Figure 12: CE as function of focal position. Inset diagram shows the relative positions of target and focal spot.

C. Conversion efficiency dependence on laser intensity

There are basically two ways to determine CE as function of laser intensity. The first is to make use of the results from CE as function of focal position. The intensity dependence can be determined because we have a map of the laser beam size in the vicinity of the focal region. Since the beam size and the laser energy are known, the laser intensity can be calculated. The other way is to position the target at a specific position whose beam size is known, while the laser energy is varied. The results from three experiments are shown in Fig. 13. One of the experiments employed the latter method in varying the laser intensities. It allowed a tighter scan through intensities in the region where optimum CE was located.

From these results, we have pinpointed the range of optimum laser intensities for producing the highest CE: 1 – 1.5 x 10^{11} W/cm^2. The CE started at a very small value in the low intensity end. As the intensity was increased, the CE also increased until it reached its peak 2%. Then it rolled off slowly after passing the optimum intensity. Towards the high intensity side ~1 x 10^{12} W/cm^2, CE dropped to very small value. This trend was also observed from the spectra as

discussed in the previous section. The optimum intensity predicted by the hydrodynamic code in Section II agrees with the experimental results, indicating the usefulness of theoretical prediction in providing insight in the source design.

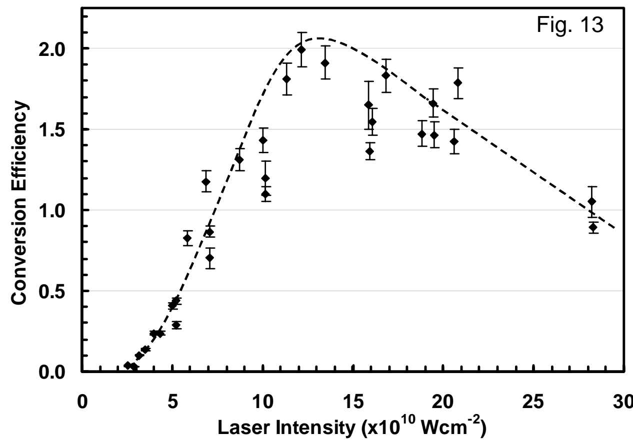

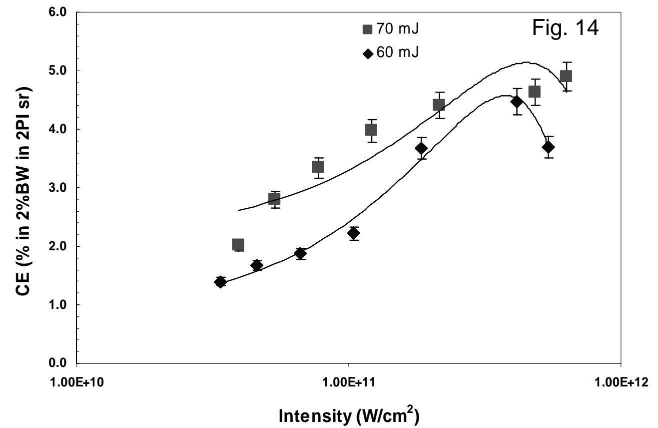

Figure 13: Conversion efficiency of the tin-doped droplet target laser plasma source as a function of laser intensity.
Figure 14: Conversion efficiency of the solid tin planar target as function of laser intensity.

In an experiment using exactly the same experimental setup as the above experiment, the tin-doped droplet target was replaced with a solid tin target of planar geometry. The laser incidence angle on the target was set at 45° with respect to the target's normal, and the FC was oriented 15° with respect to the latter. Measurements of the CE were made over a wide range of laser intensities. A mechanical device was used to carefully control the motion of the target so that, while the laser intensity at the target was kept constant, each laser shot would irradiate a fresh portion of the target. The result of the experiment (Fig. 14) shows the highest CE measured amounts to 5%.

6. CONCLUSION

A high power laser-plasma light source based on tin-doped droplet target is being developed for EUV lithography. The source technology integrates a highly efficient EUV emitter in a mass-limited target scheme. Through detailed measurements in spectroscopy and calibrated metrology on the emission of the source, the optimum laser intensity and spectral signature have been determined, thus significantly improved the source's performance, yielding maximum conversion efficiency in excess of 2% at present. With this conversion efficiency and its capability of being operated at high repetition rate, the source is capable of achieving a useful power output >50 W at the source with available laser technology. Debris studies including debris-mitigation technology are underway and are showing encouraging results as well.

ACKNOWLEDGMENTS

The authors gratefully acknowledge useful discussions with Dr. Gerard O'Sullivan from University College, Dublin; Dr. Fred Bijkerk and his team from FOM; Dr. Steve Grantham from NIST for calibrating our EUV optics; the technical support of colleagues at College of Optics and Photonics, Dr. Greg Shimkaveg, Somsak Teerawattanasook, and Joshua Duncan. This work is supported by SEMATECH and the State of Florida.

REFERENCES

1. K. Ota, Y. Watanabe, H. Franken, and V. Banine, "EUV Source Requirements," *2004 EUV Source Workshop (Miyazaki, Japan, November 2004)*

2. G. O'Sullivan and R. Faulkner, "Tunable narrowband soft x-ray source for projection lithography," *Opt. Eng*., vol. 33, pp. 3978-3983 (1994)
3. W.T. Silfvast, M.C. Richardson, H. Bender, A. Hanzo, V. Yanovsky, F. Jin and J. Thorpe, "Laser-produced plasmas for soft x-ray projection lithography", J. Vac. Sci. Technol. B 10(6), pp.3126-3133, (1992) Feng Jin, "Advanced Laser Plasma EUV Source," Ph.D. Thesis, University of Central Florida, 1995
4. R.L. Kauffman, D.W. Phillion, and R.C. Spitzer, "X-ray production ~13nm from laser-produced plasma for projection x-ray lithography applications," Appl. Opt. **32**, 6897-6900 (1993)
   R. C. Spitzer, T.J. Orzechowski, D.W. Phillion, R.L. Kauffman, and C. Cerjan, "Conversion efficiencies from laser-produced-plasma in the extreme ultraviolet regime," *J. Appl. Phys*., **79**, pp. 2251-2253 (1996)
5. Various authors, *2004 EUV Source Workshop (Miyazaki, Japan, November 2004)*
6. M. A. Klosner, and W.T. Silfvast, "Intense xenon capillary discharge extreme-ultraviolet source in the 10–16-nm-wavelength region," *Opt. Lett*., **23**, 1609 (1998)
7. F. Gilleron, M. Poirier, T. Blenski, M. Schmidt, and T. Ceccotti, "Emissive properties of xenon ions from a laser-produced plasma in the 100-140 A spectral range: Atomic-physics analysis of the experimental data," J. Appl. Phys. **94**, 2086-2096 (2003)
8. N. Bowering, M. Martins, W.N. Partlo, I.V. Fomenkov, "Extreme ultraviolet emission spectra of highly ionized xenon and their comparison with model calculations," J. App. Phys., **95**, 17 (2004)
9. I. W. Choi *et al*, "Detailed space-resolved characterization of a laser-plasma soft-x-ray source at 13.5nm wavelength with tin and its oxides," J. Opt. Soc. Am. B, **17**, 1616-1625 (2000)
10. M. C. Richardson, C-S. Koay, K. Takenoshita, C. Keyser, "High conversion efficiency tin material laser plasma source for EUVL," *J. Vac. Sci. Technol.* B, 22, 2, 785-790, (2004)
11. C-S. Koay, K. Takenoshita, E. Fujiwara, M. Al-Rabban, M. Richardson, "Spectroscopic studies of the Sn-based laser plasma EUV source," Proc. SPIE **5374**, 964-970 (2004)
12. A. Endo et al, *2004 EUV Source Workshop (Santa Clara, California, USA, February 2004)*
13. J. Pankert, *2004 EUV Source Workshop (Santa Clara, California, USA, February 2004)*
14. I. Fomenkov *et al*, *2004 EUV Source Workshop (Santa Clara, California, USA, February 2004)*
15. H. Komori *et al*, "Ion damage analysis on EUV collector mirrors," Proc. SPIE **5374**, 839-846 (2004)
16. B.A.M. Hansson and H. Hertz, "Liquid-jet laser–plasma extreme ultraviolet sources: from droplets to filaments," *J. Phys. D: Appl. Phys.* **37** (2004) 3233–3243
17. U. Stamm, "Extreme ultraviolet light sources for use in semiconductor lithography—state of the art and future development," *J. Phys. D: Appl. Phys.* **37** (2004) 3244–3253
18. F. Jin, K. Gabel, M. Richardson, M. Kado, A.F. Vassiliev, and D. Salzmann, "Mass-limited laser plasma cryogenic target for 13-nm point x-ray sources for lithography," *Proc. SPIE*, vol. 2015, pp. 151-159, (1993)
19. F. Jin, M. Richardson, G. Shimkaveg, and D. Torres, "Characterization of a laser plasma water droplet EUV source," *Proc. SPIE*, vol. 2523, pp. 81-87, (July 1995)
20. F. Jin and M. Richardson, "New laser plasma source for extreme-ultraviolet lithography," *Appl. Optics*, **34**, Issue 25, 1995, pp. 5750-5760
21. M. Richardson, D. Torres, C. DePriest, F. Jin, and G. Shimkaveg, "Mass-limited, debris-free laser plasma EUV source," *Optics Comm*., **145**, pp. 109-112 (1998)
22. G. Schriever, M. Richardson and E.Turcu, (submitted for publication)
23. C. Keyser, G. Schriever, M. Richardson and E.Turcu, "Studies of high-repetition-rate laser plasma EUV sources from droplet targets," *Appl. Phys. A* **77**, 217–221 (2003)
24. G.D. Kubiak, L.J. Bernardez, K. Krenz, "High-power extreme ultraviolet source based on gas jets," *Proc. SPIE*, vol 3331, 1998, pp. 81-89
25. B.A.M. Hansson, L. Rymel, M. Berglund, and H.M. Hertz, "A liquid-xenon-jet laser-plasma X-ray and EUV source," *Microelectronic Eng.* **53**, 667-670 (2000)
26. R.C. Constantinescu, J. Jonkers, P. Hegeman, and M. Visser, "A laser generated water plasma source for extreme-ultraviolet lithography and at wavelength interferometry," *Proc. SPIE*, vol. 4146, 101-112 (2000)
27. S. Dusterer, H. Schwoerer, W. Ziegler, C. Ziener, and R. Sauerbrey, "Optimization of EUV radiation yield from laser-produced plasma," *App. Phys. B*, **73**, 693-698 (2001)
28. U. Vogt, H. Stiel, I. Will, M. Wieland, T. Wilhein, P.V. Nickles, and W. Sandner, "Scaling-up a liquid water jet laser plasma source to high average power for Extreme Ultraviolet Lithography," *Proc. SPIE*, vol. 4343, 87-93 (2001)

29. H. Shields *et al*., “Xenon target performance characteristics for laser-produced plasma EUV sources,” *Proc. SPIE,* vol. 4688, 94 (2002)
30. S. Ter-Avetisyan *et al*., “Efficient extreme ultraviolet emission from xenon-cluster jet targets at high repetition rate laser illumination,” *J. App. Opt.* **94**, 5489 (2003)
31. H. Komori *et al*., “Laser-produced light source development for extreme ultraviolet lithography,” *J. Vac. Sci. Tech. B* **21**, 2843 (2003)
32. First mentioned in a report by JMAR Research Corp.at the EUVL Source Workshop , March 2, 2001, Santa Clara, CA
33. K. Takenoshita, C-S. Koay, M. Richardson, I.C.E. Turcu, “The Repeller Field debris mitigation approach for EUV sources”, *Proc. SPIE*, vol. 5037, pp. 792-800 (2003)
34. K. Takenoshita, C-S. Koay, S. Teerawattanasook, M. Richardson, “Debris studies for the tin-based droplet laser-plasma EUV source,” *Proc. SPIE*, vol. 5374 (2004)
35. M. Richardson, “Laser plasma EUVL sources: progress and challenges,” *Proc. SPIE* **5374**, (2004)
36. P.A.C. Jansson, B.A.M. Hansson, O. Hemberg, M. Otendal, A. Holmberg, J. de Groot, and H.M. Hertz, “Liquid-tin-jet laser-plasma extreme ultraviolet generation,” *Appl. Phys. Lett*. **84**, 2256-2258 (2004)
37. T. Tomie et al, “Particle-cluster tin target for a high conversion efficiency LPP source for EUVL,” *Proc. SPIE* **5374**, 383-393 (2004)
38. Authors: U. Stamm (XTREME Technologies); J. Pankert (Phillips); B. Hansson (Innolite); *2003 EUV Source Workshop (Santa Clara, California, USA, February 2003)*
39. JMAR laser, diode-pumped 5000W, 100kHz or Northrop-Grumman laser (formerly TRW-CEO laser), diode-pumped Nd:YAG, 4500W, 5kHz
40. C. Bauche-Arnoult and J. Bauche, “Statistical approach to the spectra of plasmas,” Physica Scr. **T40**, 58-64 (1992) and references therein.
41. W. Svendsen and G. O’Sullivan, “Statistics and characteristics of xuv transition arrays from laser-produced plasmas of the elements tin through iodine,” Phys. Rev. A, **50**, 3710-3718 (1994)
42. G. M. Zeng, H. Daido, K. Murai, M. Nakatsuka, and S. Nakai, “Line x-ray emissions from highly ionized plasmas of various species irradiated by a compact solid-state lasers,” J. Appl. Phys. **72**, 3355-3362 (1992)
43. P.A. Rodgers, A.M. Rogoyski, and S. J. Rose, *MED101: a laser-plasma simulation code.* User guide (Appleton, Rutherford, N.J., 1989)
44. R.D. Cowan, “The Theory of Atomic Spectra,” (Berkeley, CA: University of California Press)
45. M. Richardson *et al*, *2003 EUV Source Workshop (Antwerp, Belgium, September 2003)*
46. R. Stuik, F. Scholze, J. Tummler, and F. Bijkerk, “Absolute calibration of a multilayer-based XUV diagnostic,” *Nuclear Inst. Method Phys. Res. A*, **429**, 305-316 (2002)
47. W. Schwanda, K. Eidmann, and M.C. Richardson, “Characterization of a flat-field grazing-incidence XUV spectrometer,” *J. X-ray Sci. and Tech*., vol. 4, pp. 8-17 (1993)
48. X-ray CCD camera model: PI-SX:512 from Princeton Instrument
49. International Radiation Detection (California, USA)
50. Based upon calculation at http://www-cxro.lbl.gov/
51. S.A. van der Westen, C. Bruineman, F. Bijkerk, and V. Bakshi, “Flying Circus 2: Calibration of an Extreme Ultraviolet Source at PLEX LLC,” International SEMATECH Technology Transfer #04024490A-TR (2004), available at http://www.sematech.org